INSTITUTE OF PHYSICS PUBLISHING PHYSICS IN MEDICINE AND BIOLOGY

Phys. Med. Biol. **46** (2001) 167–181 www.iop.org/Journals/pb PII: S0031-9155(01)13688-2

Optical properties of porcine skin dermis between 900 nm and 1500 nm

Y Du[1], X H Hu[1,3], M Cariveau[2], X Ma[1], G W Kalmus[2] and J Q Lu[1]

[1] Department of Physics, East Carolina University Greenville, NC 27858, USA
[2] Department of Biology, East Carolina University Greenville, NC 27858, USA

E-mail: hux@mail.ecu.edu

Received 2 May 2000, in final form 19 October 2000

Abstract

The weak absorption of shortwave infrared light by skin tissues between 700 and 1500 nm offers an important window for diagnosis by optical means. The strong scattering of shortwave infrared light by the skin, however, presents a challenge to the modelling of light propagation through the skin and the understanding of skin optics. We have measured the collimated and diffuse transmittance and diffuse reflectance of porcine skin dermis samples within 30 h post-mortem. Monte Carlo simulations have been performed to inversely determine the absorption coefficient, scattering coefficient and anisotropy factor of the dermis samples in the spectral range from 900 to 1500 nm. We further analyse the sensitivity of the values of the parameters to the experimental errors and inverse calculation procedures. The state of the cellular integrity of the skin samples following optical measurements was verified using transmission electron microscopy. These results were correlated to study post-mortem effects on the *in vitro* optical properties of porcine dermis. We concluded that for samples stored within crushed ice for up to 30 h post-mortem the wavelength dependence of optical properties of the dermis remains unchanged while the values of the parameters vary moderately due to modification of the water content of the tissue.

1. Introduction

Unlike visible light, shortwave infrared (SWIR) light between 700 and 1500 nm can penetrate deeply into the skin; it therefore offers a potential spectral window for functional imaging and medical monitoring without the hazards of ionizing radiation. A fundamental challenge in achieving medical application of SWIR light is to understand the relation between the optical response of the skin and its structural features. Light propagation in a strongly turbid system such as the skin can be accurately analysed at macroscopic levels by a differential-integral equation of radiation transfer based on the law of conservation of energy (Chandrasekhar 1950).

[3] Author to whom correspondence should be addressed.

While the radiative transfer equation may be analytically solved for a few cases with simple boundary conditions, various approximations have to be resorted to, to obtain light distributions in problems with realistic boundary conditions. The radiative transfer modelling of light propagation can be statistically realized through Monte Carlo simulations when investigating light interaction within a turbid system (Wilson and Adams 1983, Keijzer *et al* 1989). Within the framework of radiative transfer, the bulk response of the system to the radiation, assuming macroscopic homogeneity, can be characterized using three main parameters: the absorption coefficient μ_a, the scattering coefficient μ_s and an anisotropy factor $g = \langle \cos\theta \rangle$, where θ is the scattering angle and the angled brackets represent ensemble averaging using a scattering phase function $p(\theta)$. However, these parameters cannot be directly measured, and inverse methods therefore have to be employed to calculate these parameters from experimental data. Various numerical methods based on radiative transfer theory have been used for the inverse calculation. Among these, Monte Carlo simulations provide a versatile tool for accurately modelling the light propagation in a turbid medium.

Extensive measurements have been carried out on skin in the visible and some portions of the SWIR regions to study its optical properties (Anderson and Parrish 1981, van Gemert *et al* 1989). Nevertheless, the strong scattering of light in the skin within this spectral region and the lack of efficient mathematical methods have until recently prevented accurate analysis of the propagation of light in skin and the determination of its optical parameters. The rapid progress in computer technology has enabled wide adoption of computing-intensive modelling tools such as Monte Carlo techniques. Recent studies with inverse calculations based on the Monte Carlo and adding-doubling methods, however, have only provided the optical properties of skin from the visible to SWIR regions up to 1000 nm in wavelength (Graaf *et al* 1993, Prahl *et al* 1993, Beek *et al* 1997, Simpson *et al* 1998). As a result, a significant gap exists in the database of skin optics in the SWIR region; in this region a weak water absorption band is known to exist near 1400 nm and tissue scattering is expected to decrease as the wavelength light increases. Therefore, the SWIR region provides an interesting window for understanding the interplay between water and cellular components in the optical response of the skin and may present significant opportunities for imaging the scattering-dominated skin tissues with various techniques such as optical coherent tomography (Tearney *et al* 1995). Furthermore, the same spectral region is ideal for Raman spectroscopy investigations of soft tissues since the fluorescence background is minimal for low-energy excitation photons (Baraga *et al* 1992). However, the lack of accurate optical parameters for the skin between 1000 and 1500 nm, however, has impeded thorough investigations of imaging possibilities. The present study was initiated to obtain these parameters in porcine dermis, which has been widely used as a model of the human dermis (Lavker *et al* 1991), and to study the effect of tissue structure on the parameters through their post-mortem time dependence. Even though the correlation between *in vitro* results and the *in vivo* optical response of tissue remains to be established, we expect that *in vitro* results will provide useful information for future exploration of medical imaging by optical means.

In this paper, we report our results on the *in vitro* measurements of reflectance and transmittance of porcine dermis and the inverse calculations of the three optical parameters by a Monte Carlo method. The approach here is similar to that first reported by Peters *et al* (1990) on determining optical parameters of human breast tissue. The effects of time post-mortem and different tissue storage conditions on the optical properties of the dermis have been studied through μ_a, μ_s and g. Transmission electron microscopy (TEM) was employed to find possible relations between the change in optical properties and the ultrastructure of the dermis. Furthermore, we analyse the sensitivity of the parameter values on the experimental errors and inverse calculation procedures and discuss ways to improve the accuracy of the results.

2. Experimental methods

A 30 W tungsten lamp and a monochromator (CM110, CVI Laser) with a grating ruled at 600 grooves/mm and ablazed at 1200 nm were used as a tunable light source for wavelengths from 900 to 1500 nm with a 2 nm resolution. The light output was modulated at 18 Hz by a chopper and passed through a long-pass filter to remove the second-order diffraction from the monochromator output. The light beam was collimated with a spherical lens of focal length 100 mm before incidence on the tissue sample. To measure the diffuse transmittance T_d and reflectance R_d, the scattered light signals were collected by an integrating sphere (IS-080-SF, Labsphere, Inc.) of diameter 203 mm ($2R$) with the diameters of the light entrance and exit ports reduced to 6.35 mm with port reducers. The light signal inside the integrating sphere was picked up at the detection port by an InGaAs photodiode mounted flush with the inner surface of the sphere. The photodiode was assembled with a preamplifier of 10^7 (V A^{-1}) transimpedance gain and the output signal was sent to a lock-in amplifier (SR850, Stanford Research Systems) for detection at the modulated frequency. We used a comparison method (Jacquez and Kuppenheim 1955) to determine T_d and R_d from three light measurements carried out in a sequence without removing the sample. The first (P_T) was obtained with the sample port as the entrance for the light, as shown in figure 1(a), the second (P_R) with the sample port as the exit by rotating the sphere 180° and the third (P_C) with the sample port rotated 20° from the last position so that the incident light strikes on the wall of the sphere. A built-in small baffle between the sample port and the detector port, with the same diffuse reflective coating as the wall of the sphere, prevented the photodiode from receiving light directly from the sample for the measurements of P_T and P_R. In the measurement of P_C, though, the baffle did not prevent the first reflected light from reaching the detector. Based on an analysis of light distribution inside the integrating sphere (Jacquez and Kuppenheim 1955, Pickering *et al* 1992, Du 2000), we find that T_d and R_d of the sample are given by

$$R_d = \frac{A P_R \cos 20^\circ}{A(1-f)P_C + A_s P_R \cos 20^\circ} \tag{1}$$

and

$$T_d = R_d \frac{P_T}{P_R} \tag{2}$$

where $A = 4\pi R^2$ is the total surface area of the sphere, f is the area ratio of the three ports to the sphere and $A_s = \pi(9.53)^2$ (mm^2) is the circular area of the sample exposed to the integrating sphere. The integrating sphere set-up has been calibrated against two standards of known diffuse reflectance near 80% and 50% (SRS-80-020 and SRS-50-010, Labsphere, Inc.) from 900 to 1500 nm. Based on the calibration results (Du 2000), we estimated that the experimental errors in the integrating sphere measurements of diffuse reflectance and transmittance are about ±5%.

To measure the collimated transmittance T_c, for determination of the attenuation coefficient $\mu_t = \mu_a + \mu_s$, the collimated light from the monochromator was focused with a combination of a spherical lens of focal length 400 mm and a cylindrical lens of focal length 75 mm into a rectangular spot about 4 mm × 0.5 mm at the focus (figure 1(b)). The tissue sample was placed in front of the cylindrical lens with a fully illuminated aperture of diameter 6.35 mm. A 0.5 mm slit was mounted in front of a photodiode to spatially filter the transmitted light from the sample before reaching the photodiode. An identical InGaAs photodiode and preamplifier assembly was used to collect the light signal prior to detection by the lock-in amplifier. With this set-up, and an integration time of the lock-in amplifier of as long as 30 s, we can measure a collimated transmittance as low as 8×10^{-5} with the incoherent light source. There are two

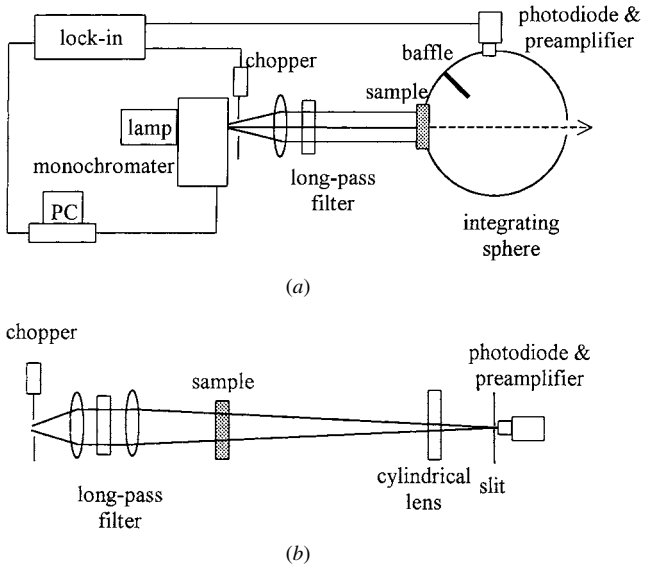

Figure 1. (*a*) The integrating sphere setup for measurements of the diffuse transmission T_d. (*b*) The spatial filtering set-up for measurements of the collimated transmission T_c.

major sources of error in determining μ_t: the 'leaking' of the scattered light through the slit of the spatial filter in the measurements of T_c for thick samples with thickness $D > 180$ μm and the thickness measurement for thin samples with $D < 100$ μm. The average error in the T_c measurements was estimated to be about $\pm 25\%$ through the measurement of the light distribution in the focal plane by scanning the slit and photodiode assembly for samples of different thickness. The sample thickness D was measured by subtracting the thickness of the sample holder from that of the sample at room temperature ($\sim$25 °C) using a micrometer of 3 μm accuracy. The micrometer has a ratchet stop mechanism which enabled us to apply a consistent measuring pressure on the tissue between measurements. A personal computer was used to control the monochromator for wavelength scanning and the lock-in amplifier for data acquisition.

Fresh porcine skin patches were obtained from the back of the neck of 6-month-old white domestic pigs at the Department of Comparative Medicine, School of Medicine, East Carolina University. Immediately after removal from the animal, the skin was kept under one of two conditions in a refrigerator: (a) within crushed ice in an ice bucket or (b) in Tyrode's physiological saline solution. The temperature in both cases was measured to be between 2 and 4 °C. For the measurement of diffuse transmittance T_d and reflectance R_d the dermis was trimmed from the porcine skin into 20 mm squares. Using a specially designed microtome, the tissue was sectioned to obtain samples of thickness D ranging from 0.48 to 1.34 mm at 4 °C in a refrigerated room. The sample was sandwiched between two sapphire optical windows of diameter 25 mm with a few saline solution drops on the sample to reduce the effect of index mismatch at the rough interface between the tissue sample and the windows. The rim of the gap between the two sapphire windows was sealed with vaseline to prevent dehydration of tissue during the measurement. For measurements of collimated transmittance T_c, however, the above sectioning method could not provide thin samples with a uniform thickness near 100 μm. Instead, we used an Ames Lab-tek cryostat to obtain dermis sections with D ranging from 30 to 250 μm at -18 °C (Lembares *et al* 1997). Each frozen tissue sample was warmed

up to room temperature in the holder and measured within 30 min of sectioning. Since the dermis is composed mainly of water and collagen fibres and the tissue was frozen in a mounting medium at optimal cutting temperature we do not expect the tissue microstructure, and thus the optical properties, to significantly change as a result of freezing (Peters *et al* 1990). Each section was examined before measurements were taken to ensure that no holes existed in the sample. A post-mortem time was defined for each sample as the period from the animal's death to the time of optical measurement or freezing in the cryostat for sectioning. All optical measurements were conducted at room temperature.

After the measurements of T_d and R_d with the integrating sphere, tissue samples were randomly selected and fixed immediately for TEM examination in 10% gluteraldehyde buffered with NaCa codylate. After fixation, samples were dehydrated in a series of alcohol solutions. The samples were then post-fixed in osmium tetroxide before infiltration with epoxy resin at 64 °C for 24 h. The resulting blocks were trimmed prior to sectioning. A Sorvall ultramicrotome was used to produce sections approximately 1 mm^2 and 60–70 μm thick with a diamond knife. The samples were contrasted with lead citrate and uranyl acetate for TEM analysis (Cariveau 2000).

3. The inverse calculations and calibration

Inverse calculations have been conducted through Monte Carlo simulations to determine the three optical parameters, μ_a, μ_s and g, from the three measured optical observables, T_c, T_d and R_d, between 900 nm and 1500 nm. The inverse calculation procedures were started by determining the attenuation coefficient $\mu_t = \mu_a + \mu_s$ at each wavelength from the collimated transmittance T_c of 36 thin dermal samples. Assuming the Lambert–Beer's law for the collimated transmittance at a fixed wavelength, $T_c(D) = A\exp(-\mu_t D)$ with A describing the loss and deflection of incident light at the surfaces of the tissue sample, the bulk attenuation coefficient μ_t can be calculated from the slope of the straight line fitted to $\log(T_c)$ versus D. An example of the fitting for two groups of samples is displayed in figure 2 at a wavelength of 980 nm. After this procedure, μ_t was used as an input parameter for the Monte Carlo simulations to find two independent parameters, μ_s and g, from the T_d and R_d measured by the integrating sphere for each sample of different thickness at each wavelength.

Using a recently developed Monte Carlo simulation method (Song *et al* 1999, Lu *et al* 1999), we calculated the reflectances and transmittances of a collimated light beam incident on a tissue phantom with a configuration identical to the experiment at wavelength λ. The values of the three optical parameters, μ_a, μ_s and g, were selected prior to the simulation subject to the condition that $\mu_a + \mu_s = \mu_t$. The two optical windows holding the tissue samples were considered and the variation of refractive index of the window material (sapphire) with the wavelength was used in the simulations while the refractive index was assumed as a constant, $n = 1.41$, for the skin dermis (Tearney *et al* 1995) because of a lack of data on the refractive index of skin. In our Monte Carlo simulations, the photons were tracked individually inside the tissue phantom until absorption or until they escaped from the tracked region (20×20 mm^2 with different sample thickness) in the tissue phantom. Since the tracked region is much larger than the illuminated region allowed by the holder aperture, the portion of the incident photons escaping from the side of the sample was expected and confirmed numerically to be negligible in comparison with the experimental errors in the T_d and R_d measurements. We adopted the Henyey–Greenstein distribution function for the scattering phase function $p(\theta)$ characterized by an anisotropy factor g (Song *et al* 1999). The probabilities of reflection and refraction of the tracked photons at the tissue–glass or glass–air interfaces were determined randomly from a distribution function determined by the Fresnel reflection coefficient for plane wave at

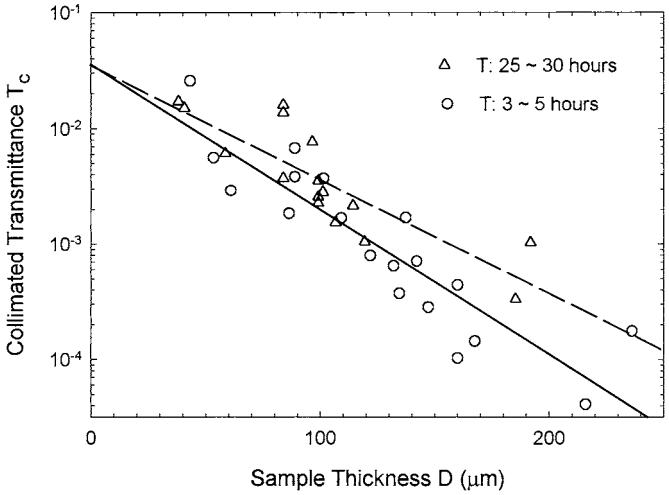

Figure 2. The collimated transmittance T_c of 36 samples versus the sample thickness D at wavelength $\lambda = 980$ nm. The samples are separated into two groups with post-mortem time $3 < T < 5$ h or $25 < T < 30$ h for fitting with the full/broken lines to obtain two different values of the attenuation coefficient μ_t from the slope of the lines.

a flat interface. When tracked photons emerged from the sample holder, they were categorized as specular reflection, collimated transmission, diffuse reflection and diffuse transmission according to their propagation direction and location at the exit surfaces and the geometry of the ports in the integrating sphere. Upon the completion of the tracking process, the total numbers of escaped photons in each category were tallied to compute the specular/diffuse reflectances and collimated/diffuse transmittances. The values of the calculated diffuse reflectance and transmittance, $(R_d)_{\text{cal}}$ and $(T_d)_{\text{cal}}$, were compared with the measured values, $(R_d)_{\text{mea}}$ and $(T_d)_{\text{mea}}$, and a total squared error function $\delta^2\ (\mu_a, \mu_s, g)$ was obtained:

$$\delta^2 = \left(\frac{(R_d)_{\text{cal}} - (R_d)_{\text{mea}}}{(R_d)_{\text{mea}}}\right)^2 + \left(\frac{(T_d)_{\text{cal}} - (T_d)_{\text{mea}}}{(T_d)_{\text{mea}}}\right)^2. \tag{3}$$

The simulation was repeated with a new set of μ_a, μ_s and g until $\delta^2\ (\mu_a, \mu_s, g) < 0.001$. With a proper choice of the three parameters, it usually took two or three iterations to achieve $\delta^2\ (\mu_a, \mu_s, g) < 10^{-4}$. We found that the statistical fluctuation in the calculated values of T_d and R_d becomes negligible when the total number of injected photons, N_0, exceeds 10^5 and therefore we chose $N_0 = 2.8 \times 10^5$ for all the simulations. To ensure the uniqueness of the inversely determined optical parameters from the experimental observables, we further calculated the total squared error function $\delta^2\ (\mu_a, \mu_s, g)$ against a large set of the two independent variables, μ_s and g, for selected samples. A typical example shown in figure 3 clearly indicates the convergence of the inverse procedure and confirms the expectation that the inverse calculation based on our Monte Carlo codes is well behaved.

To validate the inverse method, we have compared the optical parameters determined from the above procedures with the predictions based on the Mie theory and absorption coefficients based on T_c measurements for six different solutions of polystyrene microspheres. The solutions of microspheres with a diameter $2r = 0.966 \pm 0.015$ μm were diluted with distilled water from the 10% solid by weight water suspension (5095B, Duke Scientific Corp.) to three different number densities ρ_n in units of mm^{-3}: 2.03×10^6, 5.08×10^6 and 1.02×10^7. At each value of ρ_n two solutions were prepared, with pure water and with water–India ink

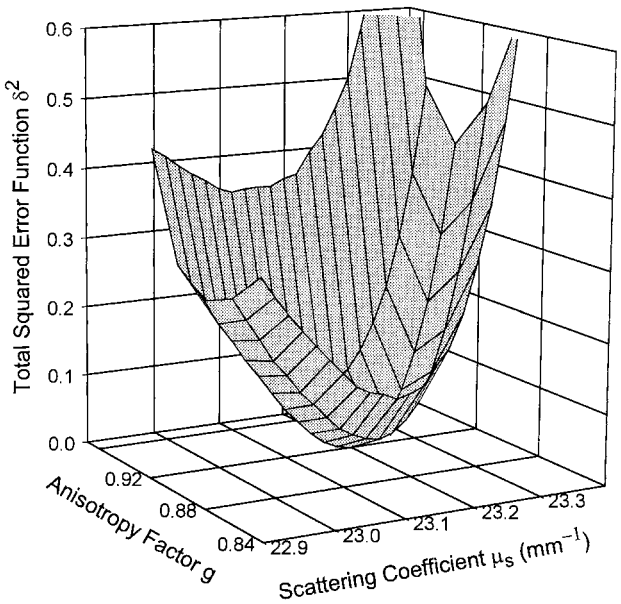

Figure 3. The total squared error function δ^2 (μ_a, μ_s, g) as a function of μ_s and g. The value of $\mu_t = \mu_a + \mu_s = 23.8$ mm^{-1} is kept as a constant while μ_s and g are varied from their optimal values determined at $\lambda = 1160$ nm for a sample stored within ice with $D = 930$ μm and $T = 3$ h.

solution, at the same ink–water concentration, to vary the absorption coefficient. For each solution, the attenuation coefficient μ_t was first determined from the T_c measurement at two sample thicknesses, 0.52 mm and 0.84 mm, followed by the R_d and T_d measurements with the sample thickness near 2.39 mm. The optical parameters of μ_a, μ_s and g were inversely determined from T_d and R_d from our Monte Carlo codes. A relative scattering cross section Q_s of the microsphere was obtained through

$$Q_s = \frac{\sigma_s}{\pi r^2} = \frac{\mu_s}{\rho_n \pi r^2}$$

where σ_s is the scattering cross section of the microspheres. We have assumed that the microspheres have negligible absorption coefficient and the water or water–ink solution has negligible scattering coefficient for light between 900 and 1300 nm. We did not extend the comparison to 1500 nm due to a lack of polystyrene absorption data near its absorption peak near 1400 nm (Matheson and Saunderson 1952).

Both Q_s and g were numerically calculated from the rigorous results of Mie theory on light scattering by spherical particles with a radius $r = 0.483$ μm (Bohren and Huffman 1983). The refractive index n of the polystyrene sphere between 900 and 1300 nm was assumed to be 1.57 by extrapolating the Cauchy dispersion formula of index, determined by the indices in the visible region, to 1000 nm (Matheson and Saunderson 1952). To assess the inversely determined μ_a, we either obtained the absorption coefficient of the same water–ink solutions without microspheres from T_c measurements based on the Lambert–Beer law or that of the pure water by Hale and Querry (1973). The inversely determined μ_a, Q_s and g are plotted against wavelength in figure 4 between wavelengths 900 and 1300 nm with mean value and standard deviation obtained from three solutions of different ρ_n with and without ink respectively. In figure 4(a), the inversely determined μ_a show good agreement with those based on T_c measurements. From figures 4(b) and (c), we find that the Q_s and g inversely determined

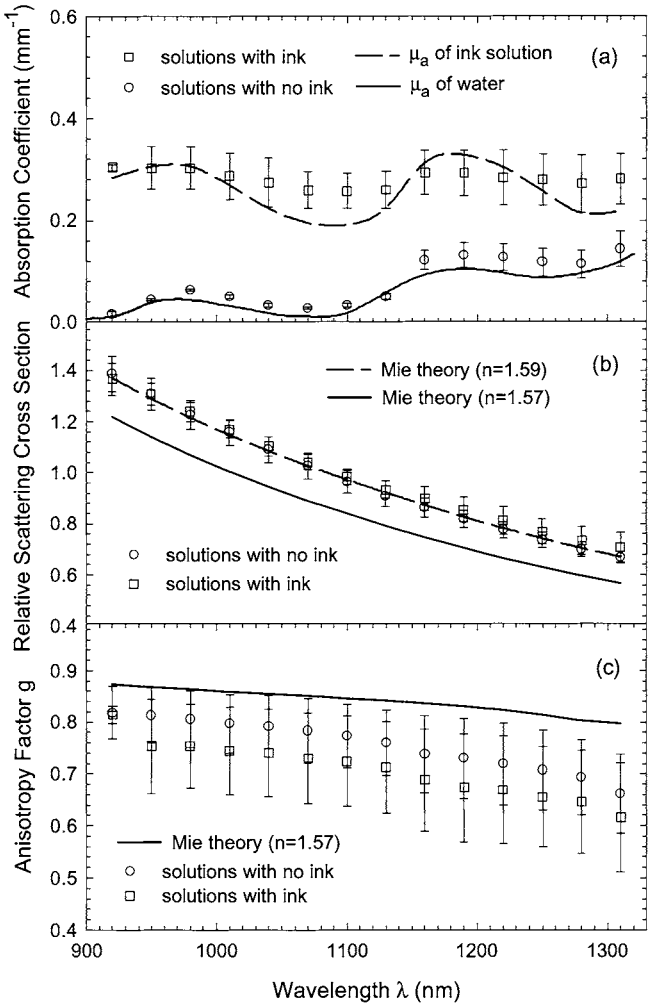

Figure 4. The wavelength dependence of the inversely determined (*a*) absorption coefficient, (*b*) relative scattering cross section and (*c*) anisotropy factor of the microsphere solutions in comparison with the absorption coefficient of water–ink solution and that of pure water (Hale and Querry 1973) based on the T_c measurements in (*a*) and Mie theory results in (*b*) and (*c*).

from six solutions agree with each other within the experimental errors and exhibit a similar wavelength dependence as that obtained using Mie theory. While the difference between the inversely determined and Mie theory results appears relatively high, 14% for Q_s and 12% for g, we should point out that the Mie theory results for Q_s are very sensitive to the refractive index of the polystyrene sphere. For example, a variation of refractive index from 1.57 to 1.59 brings the Mie theory results to overlap with the Q_s data. The increasing difference between inversely determined g and Mie theory results as the wavelength approaches 1300 nm could be attributed to the increasing light absorption by the microspheres. Based on these results and considerations, we concluded that the overall relative errors in the inversely determined optical parameters should be less than $\pm 10\%$ for the microsphere solutions.

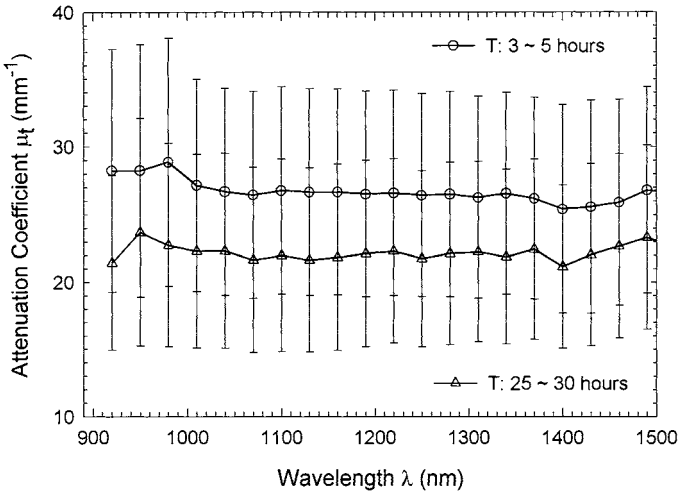

Figure 5. The wavelength dependence of the attenuation coefficient μ_t obtained from the two groups of samples with different post-mortem time T. The full lines are a guide for the eye.

4. Results

The collimated transmittance T_c was measured for 36 thin samples of porcine skin dermis at wavelengths from 900 to 1500 nm at 30 nm per step using the spatial filtering technique shown in figure 1(b). We determined the attenuation coefficient μ_t from the thickness dependence of T_c at different wavelengths. The thin samples were obtained through cryostat sectioning from tissue samples stored within crushed ice with a post-mortem time T before freezing in the cryostat. To study the effect of T on μ_t, the data from 36 samples were separated into two groups: one of 19 samples with T between 3 and 5 h and another of 17 samples between 25 and 30 h. At each wavelength the attenuation coefficient μ_t was obtained by fitting of a straight line to the experimental data for each group, as shown in figure 2. In figure 5 we plot two curves of μ_t as functions of wavelength λ for the two groups. The vertical bars represent the average errors in the μ_t and were calculated from the following equation

$$\left|\frac{\delta\mu_t}{\mu_t}\right| = \sqrt{\frac{1}{N}\sum_{i=1}^{N}\left(\left|\frac{\delta\ln(T_c)_i}{\mu_i D_i}\right|^2 + \left|\frac{\delta D}{D_i}\right|^2\right)} \tag{4}$$

where N is the number of samples for each group and $\delta\ln(T_c)_i$ is the relative error in the T_c measurement of the ith sample. The term $\delta\ln(T_c)_i$ was obtained by calculating the deviation of the measured values of T_c of the ith sample from the fitted value given by the respective straight line. The average errors in thickness measurement, $\delta D/D_i$, were determined by repeating thickness measurements for samples divided in three thickness groups: $\pm 23\%$ for samples with $D < 100\ \mu$m; $\pm 16\%$ for $100\ \mu\text{m} < D < 180\ \mu$m and, $\pm 10\%$ for $180\ \mu\text{m} < D < 270\ \mu$m. Combining these calculations we determined the relative errors in the determination of μ_t for samples in both groups to be about $\pm 30\%$.

To study the effect of storage conditions and T on the other optical parameters, we measured the diffuse transmittance T_d and reflectance R_d of 19 samples stored either within crushed ice or in Tyrode's solution with T ranging from 2 to 30 h. Monte Carlo simulations have been performed for each sample of different D to determine the value of μ_s, μ_a and g until the total squared error function δ^2 (μ_a, μ_s, g) became less than 0.001. For samples

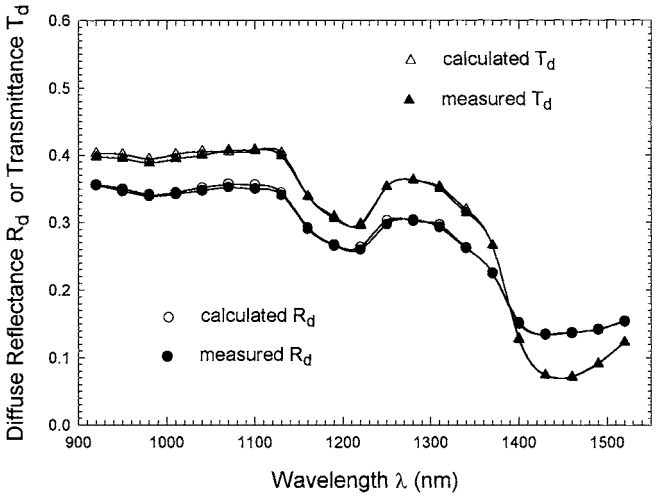

Figure 6. The measured and calculated diffuse reflectance R_d and transmittance T_d as a function of wavelength from a porcine dermis sample stored within ice with $D = 930$ μm and $T = 2$ h. The full lines are a guide for the eye.

with $T < 10$ h, the attenuation coefficients μ_t determined from the thin sample group with T between 3 and 5 h were used in the simulations, while for samples with $T > 20$ h values of μ_t from the thin sample group with T between 25 and 30 h were used. Typical results for the calculated and measured values of T_d and R_d from a sample with $T = 2$ h and $D = 930$ μm are plotted as a function of wavelength in figure 6 to demonstrate the excellent agreement between the calculated and measured values. The three optical parameters, g, normalized μ_s and μ_a, of the 19 samples are shown in figure 7 as functions of the post-mortem time T at three wavelengths of 980, 1370 and 1400 nm. No significant changes in these parameters can be identified in figure 7 for samples with different storage conditions. This suggests that storage of the skin in crushed ice for $T < 30$ h maintains the cellular integrity of the dermis, Tyrode's solution being a well known physiological saline (PBS) for tissue preservation. To confirm this conclusion, we further examined the ultrastructure of the dermal samples after the optical measurements through TEM. Again, no observable tissue changes in cells or collagen fibres were noted in the dermis with T up to 30 h (Cariveau 2000).

From figure 7, we also find that the scattering coefficient μ_s of the samples in the group with $2 < T < 10$ h displays an approximate 20% decrease from that for the group with $20 < T < 30$ h while the changes in μ_a and g are smaller. It is obvious that the relatively large difference in μ_s between samples in the two groups is a consequence of using two different values of μ_t for the inverse calculations. To reduce the fluctuations in the results between the samples, we extended the integrating sphere measurement by adding 25 porcine dermal samples stored within crushed ice. The additional samples were combined with the previous 19 samples and divided in two groups of 22 samples each according to the post-mortem time. Identical Monte Carlo simulations were performed to determine the optical parameters. Combining the results from the total of 44 fresh porcine dermal samples, we obtained the average of the optical parameters as a function of the wavelength from 900 to 1500 nm for each group of samples with different T (figure 8). The error bars represent the standard deviation of the respective optical parameters for the samples within each group.

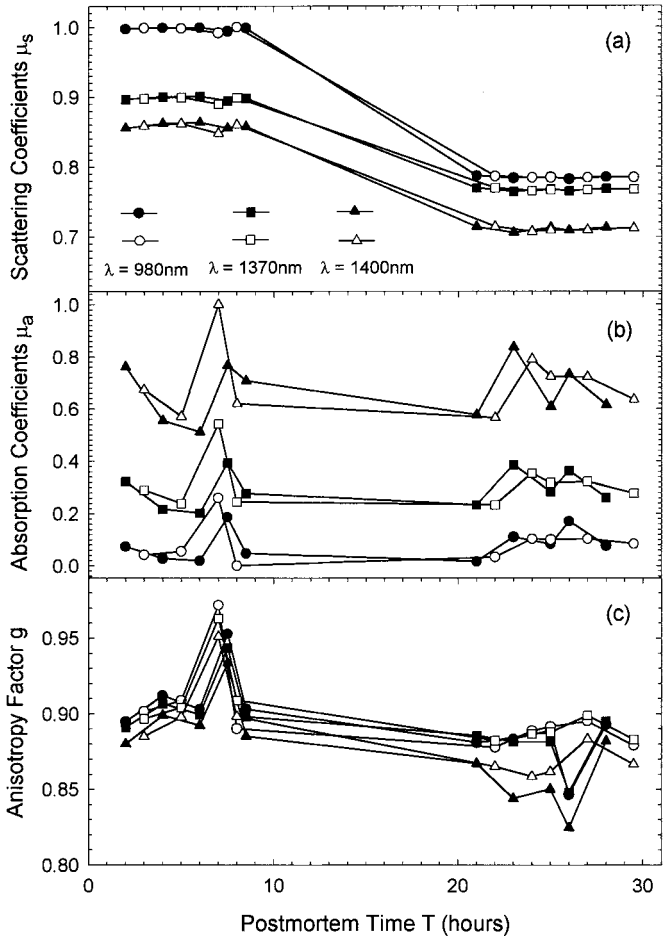

Figure 7. The optical parameters inversely determined for 19 skin dermis samples with different post-mortem time and storage conditions at three wavelengths. The full symbols are for the samples stored within ice and the open symbols are for samples in Tyrode's solution: (*a*) the scattering coefficients are normalized to $\mu_{s\_\max} = 28.9\ (\mathrm{mm}^{-1})$; (*b*) the absorption coefficients are normalized to $\mu_{a\_\max} = 0.92\ (\mathrm{mm}^{-1})$; (*c*) the anisotropy factor. The full lines are a guide for the eye.

5. Discussion

The lack of experimental data on the optical parameters of skin in the important SWIR spectral region from 900 to 1500 nm has motivated us to construct the current experimental set-ups and perform our first measurements on porcine skin dermis. The weak absorption band for water near 1400 nm provides a unique opportunity to study the role of water in skin optics. The choice of porcine skin was made because of the similarity between the tissue structures of porcine and human skin (Lavker *et al* 1991) and the relative ease in obtaining a large number of samples for investigations of the optical properties of the skin dermis and the possible effect of post-mortem alterations.

The theoretical framework of this study is provided by radiative transfer theory within which Monte Carlo simulations were applied for accurately inverting the measured reflectance

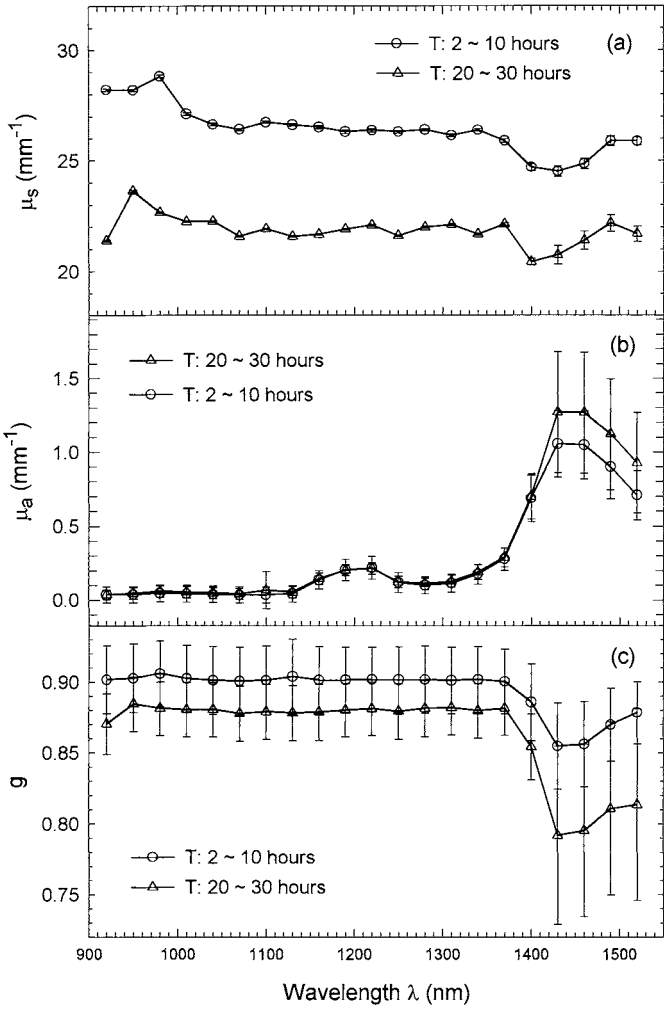

Figure 8. The averaged wavelength dependence of (*a*) the scattering coefficient μ_s, (*b*) the absorption coefficient μ_a and (*c*) the anisotropy factor g for 44 porcine skin dermis samples with post-mortem time $T < 30$ h. The error bars represent the standard deviation of the parameter within the sample group. The full lines are a guide for the eye.

and transmittances to obtain the three optical parameters μ_a, μ_s and g. To asses the validity of our method, we have analysed the sensitivity of the values of the parameters on the experimental errors and inverse calculation procedures by calculating the total squared error δ^2 (μ_a, μ_s, g) as a function of individual variations in the optical parameters. In figure 9 we show the variations of δ^2 (μ_a, μ_s, g) due to fractional changes in one of the three parameters, μ_a, μ_s and g, from their optimal values calculated for two different samples. It becomes clear from figure 9 that the accuracy of the inverse calculation is most sensitive to changes in the anisotropy factor g and least sensitive to changes in the absorption coefficient μ_a. In fact, a $\pm 6\%$ change in μ_a would still satisfy the tolerance requirement that $\delta^2 < 0.001$ for sample #1, revealing the large uncertainty in determining the absorption coefficient in a strong scattering medium of the skin dermis. By contrast, a mere $\pm 0.4\%$ change in the anisotropy factor g causes the total squared

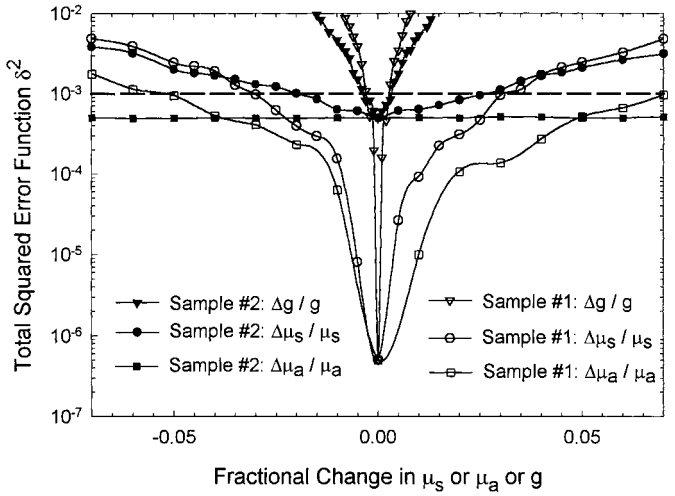

Figure 9. The total squared error function δ^2 (μ_a, μ_s, g) as a function of fractional change in one of μ_a, μ_s and g from their optimal values for two samples. The measured values of T_d and R_d were obtained at $\lambda = 1220$ nm for sample #1 with $D = 930$ μm and $T = 3$ h and at $\lambda = 1070$ nm for sample #2 with $D = 678$ μm and $T = 3$ h. The broken line indicates the maximum tolerance of the inverse calculation and the full curves are a guide for the eye.

error for sample #1 to exceed 0.001 because the choice of g strongly affects the simulated light distribution on two sides of the slab sample. These results indicate that assuming g as a constant in the determination of the wavelength dependence of optical parameters of skin tissues (Simpson *et al* 1998) could add a significant source of error in calculating μ_a and μ_s. Comparing the same analysis applied to two different samples in figure 9, we note that the minimum values of the total squared error, $\delta^2_{\min}$, differ by three orders of magnitude. The value of $\delta^2_{\min}$ indicates the inconsistency between the values of $(T_d)_{\text{mea}}$ and $(R_d)_{\text{mea}}$ and the difference in $\delta^2_{\min}$ can be attributed to the variation of the experimental errors between the measurements. For all the inverse calculations performed for the 44 samples, we found that they all produced $\delta^2_{\min}$ of less than 0.001, or $\sqrt{\delta^2_{\min}} < 3\%$, which is smaller than the estimated error of $\pm 5\%$ in the measurements of T_d and R_d. Furthermore, we would like to point out that the relatively large experimental error in determining μ_t from the T_c versus D measurements has a comparatively small effect on the inverse calculations due to the insensitivity of δ^2 (μ_a, μ_s, g) to μ_a and μ_s. Based on this observation, and the fact that a large number of samples were used in the integrating sphere measurements, we anticipated that our inverse procedures yield consistent values of optical parameters; this was confirmed by the small statistical fluctuations in μ_a and μ_s as shown in figure 8.

From the wavelength dependence of the optical parameters of porcine dermis, shown in figure 8, one can clearly see that the response of the dermis to SWIR light is dominated by scattering since μ_s is an order of magnitude larger than μ_a. As expected, the anisotropy factor $g = \langle \cos\theta \rangle$ remains approximately constant at around 0.9 between 900 and 1370 nm, indicating the strong forward nature of the light scattering by the dermis. The absorption coefficient μ_a displays a peak between 1400 and 1500 nm which can be associated with the light absorption by water (Hale and Querry 1973). The similar increases of the absorption coefficient μ_a from 1310 to 1430 nm, a factor of 10 in the porcine dermis versus a factor of near 40 in water, suggests that the absorption by the dermis is mainly due to its water component.

It also noted that the anisotropy factor g exhibits a significant decrease near 1430 nm which is not an artefact of simulations but is directly supported by the experimental observation of R_d becoming larger than T_d between 1400 and 1500 nm as displayed in figure 6. The correlation between μ_a and g is not well understood at this time.

An unexpected result lies in the difference between the optical parameters of two sample groups with different post-mortem times T. While we observed no significant changes in cellular morphology and collagen fibres in samples stored within crushed ice or in Tyrode's solution for $T < 30$ h by TEM, we found that tissue samples stored within ice exhibited signs of hydration as T approaches 30 h. Furthermore, the wavelength dependences of the parameters obtained from the two sample groups closely resemble each other. These facts indicate to us that the difference should be attributed to the change in the water content of the skin samples. This conclusion is further manifested by the near overlapping of the two curves of $\mu_a(\lambda)$ for $\lambda < 1370$ nm in figure 8(b) which separate only around the peak of the water absorption band near 1430 nm.

We note two deficiencies in the current procedure. First, the effect of surface roughness of the sectioned tissue samples has not been taken into account in the inverse calculations. This leads to the overestimate of the scattering coefficient because the deflection of the incident light at the two surfaces of the sample is treated as a part of bulk scattering. Second, we assumed the average refractive index of the tissue to be a constant, $n = 1.41$, over the spectral region from 900 to 1500 nm. The value of n has not been verified experimentally for the dermis and, in any case, the assumption of n as a constant is not a good approximation in studying the light deflection due to the index mismatch at the tissue surfaces. Current investigations are under way to address these concerns quantitatively.

In summary, we have conducted optical measurements of skin dermis in the spectral region from 900 nm to 1500 nm and determined the scattering coefficient μ_s, the absorption coefficient μ_a and the anisotropy factor g within the framework of the radiative transfer theory. Moreover, we have investigated the effect of the tissue storage conditions and post-mortem time on the optical response of the skin tissue to SWIR light. We conclude that no significant changes occur in the tissue architecture of the porcine dermis for samples stored within crushed ice for up to 30 h. The values of the scattering coefficient and anisotropy factor, however, were found to change as a result of sample hydration during storage within crushed ice.

Acknowledgments

Some of the numerical simulations were performed on Origin 2000 workstations through a grant from the North Carolina Supercomputing Center. The authors would like to thank A Miller for the Mietab code used in our Mie theory calculation. X H Hu acknowledges support through a research grant from the National Institute of Health (R15GM/OD55940-01) and J Q Lu acknowledges support through a research grant from the National Science Foundation (PHY-9973787).

References

Anderson R R and Parrish J A 1981 The optics of human skin *J. Invest. Dermatol.* **77** 13–19

Baraga J J, Feld M S and Rava R P 1992 *In situ* optical histochemistry of human artery using near infrared Fourier transform Raman spectroscopy *Proc. Natl Acad. Sci., USA* **89** 3473–7

Beek J F, Blokland P, Posthumus P, Aalsers M, Pickering J W, Sterenborg H J C M and van Germert M J C 1997 *In vitro* double-integrating-sphere optical properties of tissues between 630 and 1064 nm *Phys. Med. Biol.* **42** 2255–62

Bohren C F and Huffman D R 1983 *Absorption and Scattering of Light by Small Particles* (New York: Wiley) ch 4

Chandrasekhar S 1950 *Radiative Transfer* (London: Oxford University Press)

Cariveau M 2000 The interaction of optical radiation with epithelial tissue *MS Thesis* Department of Biology, East Carolina University

Du Y 2000 Optical properties of porcine dermis in the near infrared region between 900 nm and 1500 nm *MS Thesis* Department of Physics, East Carolina University

Graaff R, Dassel A C M, Koelink M H, de Mul F F M, Aarnoudse J G and Zijlstra W G 1993 Optical properties of human dermis *in vitro* and *in vivo Appl. Opt.* **32** 435–47

Hale G and Querry M 1973 Optical constants of water in the 200 nm to 200 micrometer wavelength region *Appl. Opt.* **12** 555–63

Jacquez J A and Kuppenheim H F 1955 Theory of the integrating sphere *J. Opt. Soc. Am.* **45** 450–70

Keijzer M, Jacques S T, Prahl S A and Welch A J 1989 Light distributions in artery tissue: Monte Carlo simulations for finite-diameter laser beams *Lasers Surg. Med.* **9** 148–54

Lavker R M, Dong G, Zheng P S and Murphy G F 1991 Hairless micropig skin. A novel model for studies of cutaneous biology *Am. J. Pathol.* **138** 687–97

Lembares A, Hu X H and Kalmus G W 1997 Absorption spectra of the cornea in the far ultraviolet region *Invest. Ophthalmol. Vis. Sci.* **38** 1283–7

Lu J Q, Hu X H, Song Z and Dong K 1999 Simulation of light scattering in biological tissues: the coherent component *Proc. SPIE* **3601** 474–81

Matheson L A and Saunderson J L 1952 Optical and electrical properties of polystyrene *Styrene: Its Polymers, Coplymers and Derivatives* ed R H Boundy and R F Boyer (New York: Reinhold) ch 11

Peters V G, Wyman D R, Patterson M S and Frank G L 1990 Optical properties of normal and diseased human breast tissues in the visible and near infrared *Phys. Med. Biol.* **35** 1317–34

Pickering J W, Moes C J M, Sterenborg H J C M, Prahl S A and van Gemert M J C 1992 Two integrating sphere with an intervening scattering sample *J. Opt. Soc. Am.* A **9** 621–31

Prahl S A, van Germert M J C and Welch A J 1993 An iterative adding-doubling algorithm for determining the optical properties of turbid media *Appl. Opt.* **32** 559–68

Simpson C R, Kohl M, Essenpreis M and Copes M 1998 Near-infrared optical properties of *ex vivo* human skin and subcutaneous tissue measured using the Monte Carlo inversion technique *Phys. Med. Biol.* **43** 2465–78

Song Z, Dong K, Hu X H and Lu J Q 1999 Monte Carlo simulation of converging laser beams propagating in biological tissues *Appl. Opt.* **37** 2944–9

Tearney G J, Brezinski M E, Southern J F, Bouma B E, Hee M R and Fujimoto J G 1995 Determination of the refractive index of highly scattering human tissue by optical coherence tomography *Opt. Lett.* **21** 2258–60

Wilson B C and Adams G 1983 A Monte Carlo model for the absorption and flux distributions of light in tissue *Med. Phys.* **10** 824–30

van Gemert M J C, Jacque S L, Sterenborg H J C M and Star W M 1989 Skin optics *IEEE Trans. Biomed. Eng.* **36** 1146–54